Material Anisotropy Revealed by Phase Contrast in Intermittent Contact Atomic Force Microscopy

Matthew S. Marcus,[1] Robert W. Carpick,[2] Darryl Y. Sasaki,[3] and M. A. Eriksson[1]

[1]*Physics Department, University of Wisconsin–Madison, Madison, Wisconsin 53706-1390*

[2]*Department of Engineering Physics, Materials Science Program, and Rheology Research Center, University of Wisconsin–Madison, Madison, Wisconsin 53706-1687*

[3]*Biomolecular Materials and Interface Science Department, Sandia National Laboratories, Albuquerque, New Mexico 87185-1413*

(Received 17 August 2001; published 17 May 2002)

Phase contrast in intermittent-contact atomic force microscopy (AFM) reveals in-plane structural and mechanical properties of polymer monolayers. This is surprising, because measurements of nanoscale in-plane properties typically require contact mode microscopies. Our measurements are possible because the tip oscillates not just perpendicular but also parallel to the sample surface along the long axis of the cantilever. This lateral tip displacement is virtually universal in AFM, implying that any oscillating-tip AFM technique is sensitive to in-plane material properties.

DOI: 10.1103/PhysRevLett.88.226103 PACS numbers: 68.47.Pe, 07.79.Sp, 68.35.Af, 68.37.Ps

Materials with highly anisotropic properties are used in a wide array of mechanical, optical, and electronic applications. Recently, anisotropic properties have been studied at the nanometer scale with atomic force microscopy (AFM) [1–6]. Measuring anisotropies with AFM requires breaking the rotational symmetry of the tip-sample interaction. Most studies of in-plane anisotropies have been conducted with lateral force microscopy (LFM), in which the tip-sample rotational symmetry is broken by the scan direction. LFM, however, is a contact-mode technique. Studies of soft materials must avoid it in favor of intermittent-contact (IC) AFM. A symmetry-breaking tip-surface interaction for IC AFM would enable nanoscale measurements of in-plane properties.

We report that phase contrast in IC AFM images is directly correlated with the in-plane anisotropy of poly(diacetylene) (PDA) monolayers. The phase shifts we observe depend on the orientation of the cantilever relative to the in-plane polymer backbone orientation of the PDA. These phase shifts arise from energy dissipation due to in-plane dissipative forces which in turn are due to tip motion parallel to the surface. Such motion is not included in current interpretations of IC AFM, which consider only one-dimensional motion of the tip perpendicular to the surface [7–10]. By symmetry, such models will not be sensitive to in-plane properties [11]. Because the cantilever is tilted relative to the plane of the sample in virtually all AFMs (11° in our case), its oscillation breaks the tip-sample rotational symmetry and enables measurement of in-plane anisotropies.

PDA monolayer films were prepared on a mica substrate using a Langmuir deposition technique [12]. PDA monolayers exhibit strong anisotropy that is correlated with their aligned polymer backbone structure [Fig. 1(a) inset] [12–15]. For example, friction measured with LFM is 3 times larger when sliding perpendicular vs parallel to these backbones [12–15], which is likely due to anisotropy in the monolayer's inelastic shear deformation modes [13].

Figure 1(a) shows an IC AFM topographic image of a PDA film with large monolayer regions. The experimental parameters are in Ref. [16]. Islands of multilayer PDA are also visible. The monolayer regions are polycrystalline, and each domain can be identified by the orientation of the striations visible in the phase image along which the PDA backbones lie [12,17]. The typical phase ϕ in Fig. 1(b) is approximately 116° [18]. Surprisingly, the phase ϕ differs from domain to domain by up to 2° in Fig. 1(b). The maximum phase $\phi_{\max}$ occurs when the long axis of the cantilever is parallel to the striations ($\theta = 0°$).

Phase shifts between the drive and the response in IC AFM indicate energy loss. In IC AFM, the cantilever's base is driven with a small amplitude, resulting in a larger tip oscillation, of order 15 nm peak to peak in our case. Cleveland *et al.* [19] have shown that, if the tip's motion is nearly sinusoidal, the power dissipated due to the

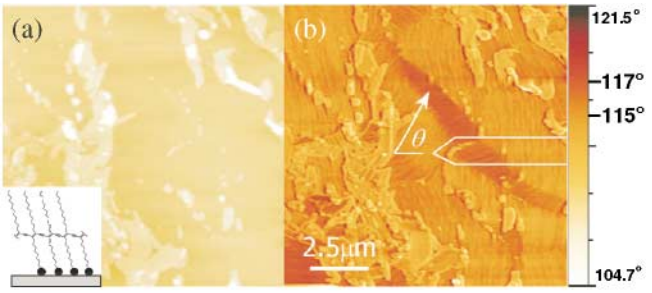

FIG. 1 (color). (a) Topographic IC AFM image of a PDA thin film acquired in constant amplitude mode. The inset shows the PDA structure and its backbone. (b) Simultaneously acquired phase contrast image. θ is the angle between the local PDA backbone striations and the long axis of the cantilever.

tip-sample interaction is well described by

$$\overline{P}_{\text{tip}} = \frac{1}{2}\frac{kA^2\omega_0}{Q}\left(\frac{A_0}{A}\sin(\phi) - 1\right), \qquad (1)$$

where k is the cantilever stiffness, A_0 is the free amplitude of oscillation, A is the amplitude during imaging, ω_0 is the angular frequency of the cantilever, Q is the quality factor of the free cantilever, and ϕ is the phase of the oscillation relative to the drive.

From Eq. (1), the phase shifts in Fig. 1(b) indicate variations in the dissipated power. Because the overall phase in Fig. 1(b) is larger than 90°, and the amplitude is held constant, an *increase* in phase ϕ corresponds to a *decrease* in the power dissipated. Thus, Fig. 1(b) shows that the power dissipated is smallest when the striations are parallel to the long axis of the cantilever. Using Eq. (1) and our system parameters [16], we find that the cantilever loses an extra amount of energy $\Delta E \approx 2.4$ eV per cycle in domains where the striations are perpendicular, rather than parallel to the long axis of the cantilever.

A simple model for an in-plane anisotropic tip-sample interaction force $F_{\text{in-plane}}$ is an isotropic dissipative force F_1, plus an anisotropic term that varies as $\sin(\theta)$ with maximum value F_2:

$$F_{\text{in-plane}} = F_1 + F_2|\sin(\theta)|, \qquad (2)$$

where θ is defined in Fig. 1(b). Equation (2) accurately describes the anisotropic friction force between PDA monolayers and LFM tips [13], where it was found that $F_2 \approx 2F_1$.

If Eq. (2) describes the dissipation, the difference in $F_{\text{in-plane}}$ between two domains will be proportional to $\Delta|\sin(\theta)| \equiv |\sin(\theta_2)| - |\sin(\theta_1)|$. The difference in power dissipated between two domains from Eq. (1) is proportional to $\Delta\sin(\phi) \equiv \sin(\phi_2) - \sin(\phi_1)$, because the amplitude A is constant. Figure 2 is a plot of $\Delta\sin(\phi)$ vs $\Delta|\sin(\theta)|$ for the data in Fig. 1. Remarkably, we find that $\Delta\sin(\phi)$ is proportional to $\Delta|\sin(\theta)|$, with proportionality constant $\alpha = (1.58 \pm 0.05) \times 10^{-2}$. This linear proportionality can be understood by considering the tip's motion. While interacting with the surface, the tip moves laterally in the plane of the surface for a distance δ. If we assume that δ is nearly independent of the domain orientation, the work done by in-plane dissipative forces is simply proportional to $F_{\text{in-plane}}$. Thus, the difference in the work done between domains is proportional to $\Delta F_{\text{in-plane}}$, which is proportional to $\Delta|\sin(\theta)|$ by Eq. (2). Power is the work done per cycle multiplied by the cantilever oscillation frequency, so we conclude that indeed $\Delta\sin(\phi) \propto \Delta|\sin(\theta)|$. Because $F_{\text{in-plane}}$ does change from domain to domain, δ might be expected to depend on domain orientation. In fact $F_{\text{in-plane}}$ is relatively small, so the lateral motion δ is *nearly constant* in our experiment, independent of domain orientation.

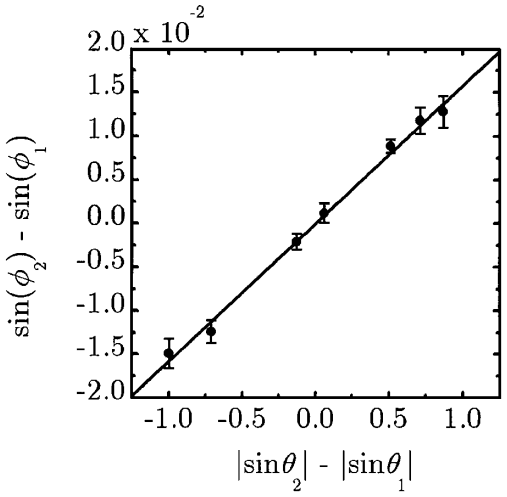

FIG. 2. The difference in the sines of the phase angles ϕ, proportional to the difference in energy loss between domains, versus the difference in the absolute values of the sines of the angles θ, proportional to the difference in the in-plane tip-sample dissipative forces. The line is $\Delta\sin(\phi) = \alpha\Delta\sin(\theta)$ with $\alpha = (1.58 \pm 0.05) \times 10^{-2}$. Data are extracted from Fig. 1.

We have assumed that the component of the tip oscillation parallel to the surface is the important symmetry-breaking motion. In principle, this need not be true, because the raster scan also causes lateral tip motion. The phase data in Fig. 3, however, demonstrate that lateral motion due to the raster scan has no effect on the data presented here. Figures 3(a) and 3(b) were acquired with the fast scan direction perpendicular and parallel to the long axis of the cantilever, respectively. Figures 3(c) and 3(d) are plots of $\Delta\sin(\phi)$ vs $\Delta|\sin(\theta)|$ corresponding to the data in 3(a) and 3(b), fit with the line $\Delta\sin(\phi) = \alpha\Delta|\sin(\theta)|$. The slopes α are the same within the fitting

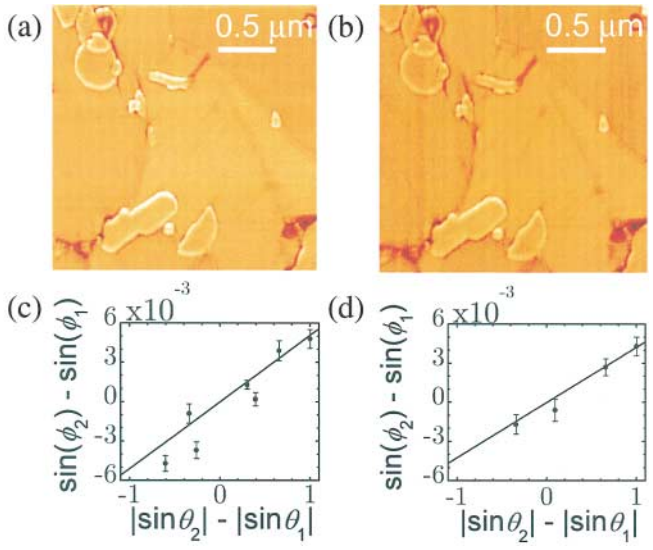

FIG. 3 (color). (a) Phase image with the fast scan axis parallel to the cantilever axis, and (b) phase color image with the fast scan axis perpendicular to the cantilever axis. (c) Correlation between energy loss difference and difference in dissipative forces for image (a). The line is $\Delta\sin(\phi) = \alpha\Delta\sin(\theta)$ with $\alpha = (5.1 \pm 1.1) \times 10^{-3}$. (d) Corresponding correlation for image (b). The line corresponds to $\alpha = (4.2 \pm 0.7) \times 10^{-3}$.

uncertainty, demonstrating that the in-plane component of the cantilever oscillation is the important symmetry-breaking interaction.

The data in Figs. 1–3 provide a measurement of surface anisotropy. The two candidates for this anisotropy are shear deformation and friction, which in fact must both be present here. Because the tip is moving at a finite lateral velocity with respect to the sample just before contact, there will be relative motion between the tip and the sample as the tip does work on the surface to increase the surface lateral velocity to match that of the tip. Similarly, as the tip slows and reverses direction near maximum compression into the sample, at some point its lateral velocity will match that of the surface. Any degree of static friction will then require a finite shear deformation before any relative sliding resumes [20]. Friction and shear deformation are in fact closely related on the length scales considered here [21].

Figure 4 is a schematic of a simple dynamic model of IC AFM designed to explain the essential characteristics of our results. The critical feature is that the tip is constrained to move along the z' axis, which is tilted an angle $\psi = 11°$ from the sample normal. To solve for the motion of the tip, all tip-sample forces are projected onto the z' axis. Ignoring motion along x' is a good approximation, as an analysis of the cantilever indicates that the effective spring constant in the x' direction is more than 30 times larger than any other spring constant in the model [22].

The key result of this model is that the sample compression during contact now occurs along z', resulting in components of motion in both the z and the x directions (Fig. 4). The in-plane motion along x is what we have demonstrated here. The forces on the tip are (i) cantilever restoring force and a damping force due primarily to interactions with the air, both acting along the z' direction; (ii) Hertz contact force acting in the z direction; (iii) tip-sample damping along the z direction acting during contact, due to inelastic deformation along z, taken to be larger than the air damping by a factor $M = 40$ [7]; and (iv) viscous tip-sample interaction along x during contact, due to both shear deformation and friction. The cantilever is driven at its resonance frequency ω_0, giving

$$\ddot{p} + \frac{\omega_0}{Q}(\dot{p} - \dot{\zeta}) + \omega_0^2(p - \zeta) = \begin{cases} 0 & p < 0 \\ -\frac{\omega_0^2}{k}\left(\cos^{5/2}(\psi) K\sqrt{R}\, p^{3/2} + \frac{Mk\cos^2(\psi)}{Q\omega_0}\,\dot{p} + \frac{k\sin^2(\psi)}{Q_c\omega_0}\,\dot{p}\right) & p \geq 0 \end{cases}, \qquad (3)$$

where p is the distance between the tip and the sample along z', defined to be zero when the tip first touches the sample and positive when in contact. The displacement of the base of the cantilever ζ drives the cantilever on resonance: $\zeta = \zeta_0(A_0/Q)\sin(\omega_0 t)$. K is the reduced contact modulus, k is the cantilever force constant, R is the tip radius, Q is the damping due to air, and Q_c is the in-plane damping.

Using parameters appropriate for Fig. 1, see Ref. [16], our model indicates a maximum tip-sample compression of 0.27 nm along z', giving a tip-sample in-plane tip motion of $\delta = 49.9 \pm 0.1$ pm along the x direction. The time spent in contact with the surface is 0.35 μs per cycle. The distance δ is extremely small, and it is difficult to make firm distinctions between friction and shear deformation at such a small scale. The important result of the calculation is that the distance δ is virtually independent of the in-plane damping. Furthermore, our model produces a nearly sinusoidal tip motion, indicating that Eq. (1) remains valid for the tilted-cantilever geometry.

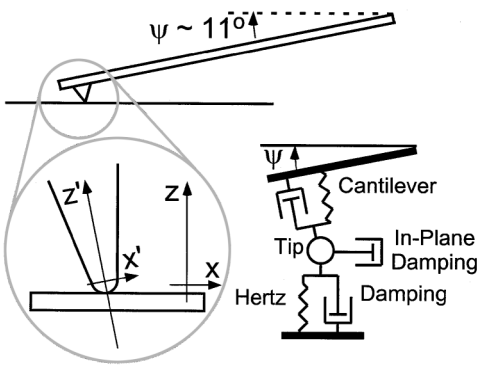

FIG. 4. Geometry of the tip-sample interaction. Cantilever oscillation occurs along the z' axis.

Phase shifts in IC AFM result from energy dissipation. However, anisotropic in-plane *elastic* forces can cause phase shift differences from domain to domain, because such forces would alter the normal penetration of the tip, changing the amount of damping. Including in-plane elasticity in our model allows us to estimate the size of this effect. The elastic in-plane stiffness of a Hertzian contact is given by $k_{\text{lat}} = 8G^*a$, where a is the contact radius and $G^* = [(2 - \nu_{\text{PDA}})/G_{\text{PDA}} + (2 - \nu_{\text{Si}})/G_{\text{Si}}]^{-1}$. G represents the respective shear moduli. For a Si-PDA interface, $G^* \cong 1$ GPa. Replacing in-plane damping with this in-plane stiffness in our model, we find that the PDA shear modulus would need to change by over an order of magnitude between the two orthogonal directions in order to cause the change in energy loss we observe (2.4 eV). Varying G_{PDA} by a more reasonable factor of 3 produces an energy loss of 0.1–0.4 eV per cycle. While in-plane elastic anisotropy may play a role, it is not the primary loss mechanism. Measurements of the amplitude and phase as a function of tip-sample displacement may allow us to quantify in-plane stiffness and sliding in the future [23–27].

There are several models of IC AFM [7–10,19,23,26, 28–30], many of which include sophisticated treatments

of adhesion and viscoelasticity—effects we have either ignored or simplified in our model. The distinguishing feature we have introduced is that the tip oscillates along an off-normal line. It is this feature that breaks the rotational symmetry of the tip-sample interaction and explains the behavior shown in Figs. 1–3.

A nonzero tilt ψ of the cantilever with respect to the sample normal is nearly universal in AFM. Increasing the tilt angle would provide greater contrast in resolving in-plane properties, as demonstrated in the shear-force mode commonly used in near-field scanning optical microscopy [14,31]. Also, the local angle ψ will change due to local variations in sample topography, contributing to contrast in any phase image, even in the case of isotropic in-plane properties. Finally, measurement of in-plane *magnetic* forces is possible using in-plane tip magnetization [32–34]. The lateral tip-sample motion we demonstrate here may allow measurements of in-plane anisotropies in other long range forces, such as electric forces.

We thank J. P. Aimé for useful discussions. We acknowledge funding from NSF Grants No. DMR0094063, No. CMS0134571, and DMR0079983, Research Corporation, and UW–Madison. Some images were prepared using WSxM (Nanotech Electronica).

[1] M. Liley *et al.,* Science **280**, 273 (1998).
[2] P. E. Sheehan and C. M. Lieber, Science **272**, 1158 (1996).
[3] H. Bluhm *et al.,* Appl. Phys. A **61**, 525 (1995).
[4] R. M. Overney *et al.,* Phys. Rev. Lett. **72**, 3546 (1994).
[5] R. Pearce and G. J. Vancso, Polymer **39**, 6743 (1998).
[6] E. Amitay-Sadovsky, S. R. Cohen, and H. D. Wagner, Appl. Phys. Lett. **74**, 2966 (1999).
[7] N. A. Burnham *et al.,* Nanotechnology **8**, 67 (1997).
[8] O. P. Behrend *et al.,* Appl. Phys. Lett. **75**, 2551 (1999).
[9] O. P. Behrend *et al.,* Appl. Phys. A **66**, S219 (1998).
[10] J. P. Spatz *et al.,* Nanotechnology **6**, 40 (1995).
[11] F. Moreno-Herrero *et al.,* Surf. Sci. **453**, 152 (2000).
[12] D. Y. Sasaki, R. W. Carpick, and A. R. Burns, J. Colloid Interface Sci. **229**, 490 (2000).
[13] R. W. Carpick, D. Y. Sasaki, and A. R. Burns, Tribol. Lett. **7**, 79 (1999).
[14] A. R. Burns and R. W. Carpick, Appl. Phys. Lett. **78**, 317 (2001).
[15] R. W. Carpick and M. Salmeron, Chem. Rev. **97**, 1163 (1997).
[16] The image was acquired with a Digital Instruments Multimode SPM and Nanoscope IIIa controller, using Si cantilevers in ambient laboratory conditions. The free amplitude $A_0 = 10.5$ nm, quality factor $Q = 560$, the excitation amplitude 19 pm, the resonance frequency $\omega_0 = 2\pi \times 271$ kHz, and damped cantilever amplitude $A = 7.7$ nm are all measurable with or controlled by the AFM controller. Note that the cantilever was driven on resonance for these experiments. The spring constant $k = 60$ N/m is the mean value of the range of spring constants specified by the manufacturer. The manufacturer's tip radius $R = 20$ nm was used for modeling purposes. The cantilever dimensions are 125 μm length, 30 μm width, 4 μm thickness, and 12.5 μm tip height. The reduced contact modulus $K = \frac{4}{3}(\frac{1-\nu_{\mathrm{Si}}}{E_{\mathrm{Si}}} + \frac{1-\nu_{\mathrm{PDA}}}{E_{\mathrm{PDA}}})^{-1} = 10.5$ GPa was calculated using the bulk values for silicon ($E = 155$ GPa, $\nu = 0.3$) and estimated values for PDA were based on measurements of hydrocarbon self-assembled monolayers.
[17] A. Lio *et al.,* Langmuir **13**, 6524 (1997).
[18] The reported phase shifts are true phase shifts with respect to the drive signal. The phase shifts reported by the instrument are not properly scaled and are shifted by 90°.
[19] J. P. Cleveland *et al.,* Appl. Phys. Lett. **72**, 2613 (1998).
[20] R. W. Carpick, D. F. Ogletree, and M. Salmeron, Appl. Phys. Lett. **70**, 1548 (1997).
[21] K. J. Wahl, S. V. Stepnowski, and W. N. Unertl, Tribol. Lett. **5**, 103 (1998).
[22] D. F. Ogletree, R. W. Carpick, and M. Salmeron (to be published).
[23] L. Nony, R. Boisgard, and J. P. Aimé, J. Chem. Phys. **111**, 1615 (1999).
[24] J. P. Aime *et al.,* J. Chem. Phys. **114**, 4945 (2001).
[25] L. Huihong and C. E. D. Chidsey, Appl. Phys. Lett. **72**, 477 (1998).
[26] F. Dubourg *et al.,* Eur. Phys. J. E **6**, 49 (2001).
[27] F. Dubourg *et al.,* Eur. Phys. J. E **6**, 387 (2001).
[28] L. Wang, Surf. Sci. **429**, 178 (1999).
[29] H. Bielefeldt and F. J. Giessibl, Surf. Sci. **440**, L863 (1999).
[30] U. Rabe, K. Janser, and W. Arnold, Rev. Sci. Instrum. **67**, 3281 (1996).
[31] A. R. Burns *et al.,* Langmuir **15**, 2922 (1999).
[32] S. H. Liou and Y. D. Yao, J. Magn. Magn. Mater. **190**, 130 (1998).
[33] L. Folks *et al.,* Appl. Phys. Lett. **76**, 909 (2000).
[34] P. Rice and S. E. Russek, J. Appl. Phys. **85**, 5163 (1999).